THE JOURNAL OF PHYSICAL CHEMISTRY A
A JOURNAL OF THE AMERICAN CHEMICAL SOCIETY

pubs.acs.org/JPCA Article

Enhancing Photogenerated Radical Pair Properties in Donor-Chromophore-Acceptor Systems for Quantum Information Applications

Paige J. Brown, Yunfan Qiu, Elisabeth I. Latawiec, Brian T. Phelan, Nikolai A. Tcyrulnikov, Jonathan R. Palmer, Matthew D. Krzyaniak, Sebastian M. Kopp, Yuheng Huang, Ryan M. Young,* and Michael R. Wasielewski*

Cite This: J. Phys. Chem. A 2024, 128, 9371−9382 Read Online

ACCESS | Metrics & More | Article Recommendations | Supporting Information

ABSTRACT: We report on new donor-chromophore-acceptor triads **BDX-ANI-NDI** and **BDX-ANI-xy-NDI** where the BDX donor is 2,2,6,6-tetramethylbenzo[1,2-*d*;4,5-*d*]bis[1,3]dioxole, the ANI chromophore is 4-(*N*-piperidinyl)naphthalene-1,8-dicarboximide, the NDI acceptor is naphthalene-1,8:4,5-bis(dicarboximide), and xy is a 2,5-xylyl spacer. The results on these compounds are compared to the analogous derivatives having a *p*-methoxyaniline (MeOAn) as the donor. $BDX^{\bullet+}$ has no nitrogen atoms and only a single hydrogen atom coupled to its unpaired electron spin, and therefore has significantly decreased hyperfine interactions compared to $MeOAn^{\bullet+}$. We use femtosecond transient absorption (fsTA) and nanosecond TA (nsTA) spectroscopies, the latter with an applied static magnetic field, to study the charge transfer dynamics and determine the spin−spin exchange interaction (J) for $BDX^{\bullet+}$-ANI-$NDI^{\bullet-}$ and $BDX^{\bullet+}$-ANI-xy-$NDI^{\bullet-}$ at both ambient and cryogenic temperatures. Time-resolved electron paramagnetic resonance (EPR) and pulse-EPR measurements on these spin-correlated radical pairs (SCRPs) were used to probe their spin dynamics. We demonstrate that $BDX^{\bullet+}$-ANI-xy-$NDI^{\bullet-}$ has an unusually long lifetime of ∼550 μs in glassy butyronitrile (PrCN) at 85 K, which makes it useful for pulse-EPR studies that target quantum information science (QIS) applications. We also show that rotation of the BDX group about the single bond linking it to the neighboring phenyl group has a significant impact on the spin dynamics, and in particular the magnitude of J. By comparing the results on these compounds to the analogous MeOAn series, insights into design principles for creating improved spin-correlated radical pair systems for QIS studies are obtained.

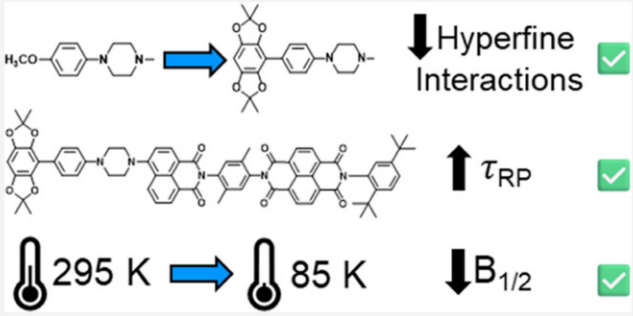

INTRODUCTION

Quantum Information Science (QIS) is a rapidly growing field that promises significant advances in computation,[1−3] communications,[4] and sensing.[5,6] In recent years, it has become apparent that molecule-based quantum bits (qubits) can be tailored synthetically to the desired application, spatially positioned with high precision, and addressed with both microwave and optical techniques.[1,7−13] Our recent work has focused on the use of photogenerated, spin-correlated radical ion pairs (SCRPs) as spin qubit pairs that fulfill the DiVincenzo criteria,[14] namely, they are initialized in a pure singlet quantum state, they have spin coherence times sufficiently long to conduct a sequence of quantum logic operations, such as a CNOT gate,[15] and the two spins can be readily addressed using selective microwave pulses.[16−19] Additionally, SCRPs can be used for quantum sensing[20] and communication protocols, such as quantum teleportation.[21]

Numerous platforms for SCRP-based spin qubits have been explored, including systems as diverse as electron donor−acceptor triads,[17,21,22] DNA hairpins,[23−25] and quantum dot - redox molecule conjugates.[26] Typical architectures of electron donor−acceptor triads include donor−acceptor(1)-acceptor(2) (D-A_1-A_2) and donor(2)-donor(1)-acceptor (D_2-D_1-A) systems in which D or A serve as the initially photoexcited chromophore, respectively. In addition, A_1 or D_1 may also function as the photoexcited chromophore (C) so that photoexcitation of the resulting donor-chromophore-acceptor (D-C-A) system produces an SCRP by one of two competitive mechanisms: D-^{1}*C-A → $D^{\bullet+}$-$C^{\bullet-}$-A → $D^{\bullet+}$-C-$A^{\bullet-}$ and D-^{1}*C-A → D-$C^{\bullet+}$-$A^{\bullet-}$ → $D^{\bullet+}$-C-$A^{\bullet-}$. The long distance between $D^{\bullet+}$ and $A^{\bullet-}$ results in a small spin−spin exchange

Received: July 25, 2024
Revised: September 29, 2024
Accepted: October 1, 2024
Published: October 16, 2024

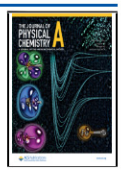

https://doi.org/10.1021/acs.jpca.4c05015
J. Phys. Chem. A 2024, 128, 9371−9382

Scheme 1. Structures of the Compounds Studied

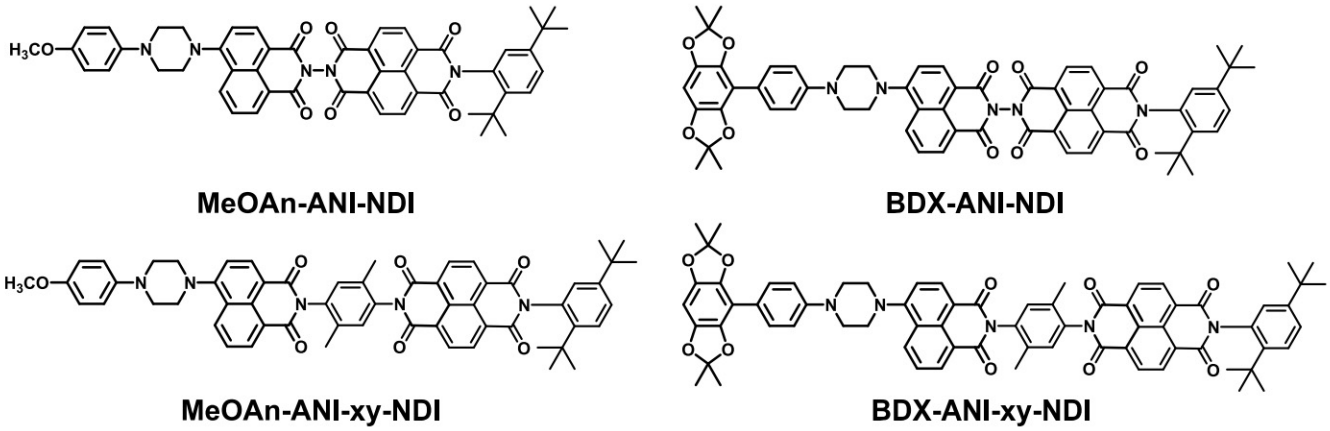

interaction (J), which permits spin evolution via zero-quantum coherence, allowing the spins to be probed by time-resolved electron paramagnetic resonance (TREPR) spectroscopies.

We have studied the prototypical D-C-A system **MeOAn-ANI-xy-NDI** extensively,[27−30] where the donor is *p*-methoxyaniline (MeOAn), the chromophore is 4-(*N*-piperidinyl)-naphthalene-1,8-dicarboximide (ANI), the acceptor is naphthalene-1,8:4,5-bis(dicarboximide) (NDI), and where ANI and NDI are linked by a 2,5-xylyl (xy) bridge. **MeOAn-ANI-xy-NDI** was first developed to demonstrate high quantum yield formation of **MeOAn$^{\bullet+}$-ANI-xy-NDI$^{\bullet-}$** to allow its observation by TREPR spectroscopy. The increasing interest in SCRPs for QIS makes **MeOAn$^{\bullet+}$-ANI-xy-NDI$^{\bullet-}$** a natural starting point for further optimizing a triad system for potential QIS applications. The linear structure of **MeOAn-ANI-xy-NDI** provides for restricting the two radical ions to a well-defined distance, where both J and the spin−spin dipolar (D) interactions are small. Moreover, ANI can be selectively excited at 410−420 nm to initiate charge separation, while the strong absorption of NDI$^{\bullet-}$ at 480 nm provides a facile wavelength to monitor the electron transfer dynamics optically.[27] Previous work by Weiss et al.[28] characterized J for **MeOAn$^{\bullet+}$-ANI-xy-NDI$^{\bullet-}$** and its shorter analog **MeOAn$^{\bullet+}$-ANI-NDI$^{\bullet-}$** by monitoring the effect of a static magnetic field on the yield of **MeOAn-ANI-xy-^{3}*NDI** and **MeOAn-ANI-^{3}*NDI**, respectively, formed by charge recombination at 295 K in toluene. Later work in fluid toluene solution showed that J is temperature dependent[29] but further explorations in the solid state at cryogenic temperatures were not conducted. The observed temperature dependence was assigned to structural changes of the piperazine bridge. Thus, the energy landscape for these D-C-A systems is highly sensitive to the environment and molecular structure in an interdependent way.

Despite the utility of **MeOAn-ANI-xy-NDI** and **MeOAn-ANI-NDI**, there are some aspects of their molecular design that could be improved for QIS applications. The hyperfine coupling constants of MeOAn$^{\bullet+}$, particularly those of its nitrogen atom and hydrogen atoms that are part of the CH_2 groups adjacent to it, can reduce the phase memory time (T_m), which is directly related to the spin coherence time (T_2),[31] and broaden the TREPR signals. Additionally, longer radical pair lifetimes and higher radical pair yields would enable studies with longer, more elaborate microwave pulse sequences, approaching the spin−lattice relaxation time (T_1) limit.

In this work, we report on new D-C-A triads with enhanced properties for QIS studies. These compounds are **BDX-ANI-NDI** and **BDX-ANI-xy-NDI**, within which the MeOAn donor in **MeOAn-ANI-NDI** and **MeOAn-ANI-xy-NDI** is replaced by 2,2,6,6-tetramethylbenzo[1,2-*d*;4,5-*d*]bis[1,3]dioxole (BDX). BDX$^{\bullet+}$ has no nitrogen atoms and only a single hydrogen atom coupled to its unpaired electron spin, and therefore has a significantly decreased hyperfine interactions compared to MeOAn. We use femtosecond transient absorption (fsTA) and nanosecond TA (nsTA) spectroscopies, the latter with an applied static magnetic field, to study the charge transfer dynamics and determine the J values for **BDX$^{\bullet+}$-ANI-NDI$^{\bullet-}$** and **BDX$^{\bullet+}$-ANI-xy-NDI$^{\bullet-}$** at both ambient and cryogenic temperatures. TREPR and pulse-EPR measurements on these SCRPs were also performed to probe their spin dynamics. We demonstrate that **BDX$^{\bullet+}$-ANI-xy-NDI$^{\bullet-}$** has an unusually long lifetime of ∼550 μs in glassy butyronitrile (PrCN) at 85 K, which makes it useful for pulse-EPR studies that target QIS applications. We also show that rotation of BDX about the single bond joining it to the neighboring phenyl group has a significant impact on the spin dynamics, and in particular the magnitude of J. By comparing the results on these compounds to the analogous MeOAn series, insights into design principles for creating improved SCRP systems for QIS studies are obtained (Scheme 1).

EXPERIMENTAL SECTION

Synthesis and Sample Preparation. **MeOAn-ANI-NDI** and **MeOAn-ANI-xy-NDI** were synthesized as previously reported but to increase solubility the terminal *n*-octyl group on the NDI was replaced with a 2,5-di-*t*-butylphenyl group.[28,32] The synthetic procedures for **BDX-ANI-NDI** and **BDX-ANI-xy-NDI** and all additional synthetic details are presented in the Supporting Information. Samples of **MeOAn-ANI-NDI**, **MeOAn-ANI-xy-NDI**, **BDX-ANI-NDI**, and **BDX-ANI-xy-NDI** for all experiments were prepared in toluene for 295 K measurements or butyronitrile (PrCN) for 85 K measurements. The sample absorbance for fsTA and nsTA measurements was 0.3−0.5 and for all other measurements was 0.5−0.7 at 415 nm. For 295 K steady-state and TA measurements, the samples were placed in a vacuum cuvette and subjected to four freeze−pump−thaw degassing cycles on a vacuum line (10^{-4} Torr) before being sealed. For low-temperature steady-state and TA experiments, the sandwich cells were loaded in a nitrogen glovebox, then placed in a Janis

https://doi.org/10.1021/acs.jpca.4c05015
J. Phys. Chem. A 2024, 128, 9371−9382

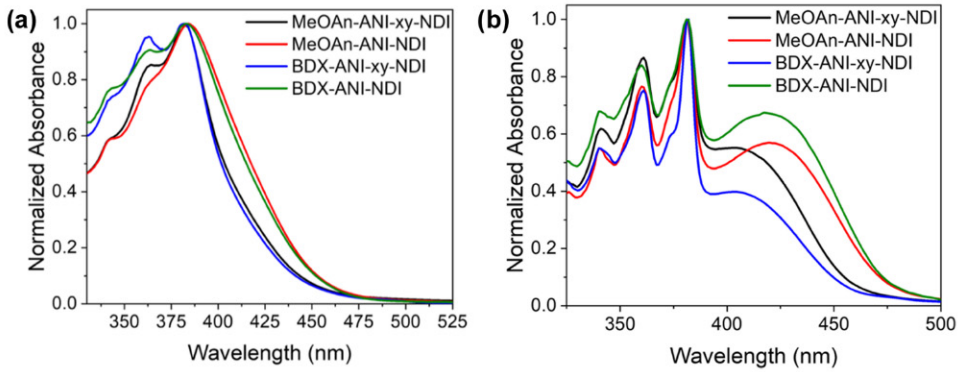

Figure 1. Normalized steady-state absorption of **MeOAn-ANI-NDI** (red), **MeOAn-ANI-xy-NDI** (black), **BDX-ANI-NDI** (green), and **BDX-ANI-xy-NDI** (blue) in toluene at 295 K (a) and in PrCN at 85 K (b).

VFN-100 cryostat. For magnetic field effect (MFE) measurements, sample solutions were loaded into rectangular borosilicate tubes (2 mm × 4 mm i.d.) and subjected to four freeze−pump−thaw degassing cycles on a vacuum line (10^{-4} Torr) and sealed using a hydrogen torch. The same protocol was used for EPR samples as described for the MFE measurements except the samples were prepared in quartz tubes (1.5 mm outer diameter, 1.00 mm inner diameter). The samples for coherence time (T_m) measurements were prepared in toluene-d_8.

Spectroscopy. *Steady-State UV−vis Absorption Spectroscopy.* The absorption spectra of **MeOAn-ANI-NDI**, **MeOAn-ANI-xy-NDI**, **BDX-ANI-NDI**, and **BDX-ANI-xy-NDI** were recorded using a Shimadzu 1800 UV−vis spectrophotometer. Measurements were carried at 85 K in a cryostat (VNF-100, Janis Research Co. LLC) using a temperature controller (Cryo-Con 32B, Cryogenics Control Systems, Inc.).

Transient Absorption Spectroscopy. Femtosecond and nanosecond transient absorption (fs/nsTA) measurements were performed as described previously.[33] For the fsTA and nsTA experiments the instrument response functions (IRF) were ∼300 fs and ∼600 ps, respectively. The output of a collinear optical parametric amplifier (TOPAS-Prime, Light-Conversion, LLC.) was depolarized to minimize polarization-specific dynamics and tuned to 414 nm and attenuated to 1 μJ/pulse.

Magnetic Field Effects. The sealed rectangular tubes were placed in a cryostat (STVP-100 Janis) positioned between the poles of an electromagnet (HV-4W and Magnion HS-735, Walker Scientific). The samples were prefrozen in liquid nitrogen before inserting them into the nitrogen-cooled cryostat at 85 K. The field strength was measured by a gaussmeter (475 DSP, Lakeshore) with a Hall effect probe. The samples were photoexcited using 415 nm, 5 ns laser pulses at a 1 kHz repetition rate output by an optical parametric oscillator pumped by the third harmonic output of a diode-pumped Nd:YAG laser (NT242, Ekspla). The white light probe pulses were generated using a 2 kHz white light supercontinuum laser (Disco 2UV, Leukos). The pump and probe pulses were combined using a 50/50 beamsplitter and focused on the sample with a 50 mm focal length lens. After passing through the sample, the probe light was collimated and coupled by a fiber optic cable into a high-speed spectrometer (Ocean FX-VIS-NIR, Ocean Optics). A laboratory-written LabVIEW program collected the raw data and calculated the shot-to-shot transient absorption difference signal. The differential nanosecond transient absorption data were collected at multiple time delays and magnetic field strengths. During the experiment, the magnetic field was controlled to $\pm 5 \times 10^{-5}$ T precision. To account for any sample degradation, the magnetic field was reset to B_0 = 0 mT every five kinetic traces. These zero points were then fit to a polynomial function in MATLAB and used to correct the observed magnetic field effect. Additional data processing details and a detailed schematic of the instrumentation can be found in the Supporting Information.

Absorption Detected Magnetic Resonance (ADMR) Spectroscopy. ADMR measurements were made using the same optical instrumentation described above for the MFE experiments. To deliver the pulsed microwaves a custom split ring resonator was constructed consisting of two concentric copper tubes (Figure S29).[34,35] The sample was placed within the inner copper tube (i.d. 6.22 mm, o.d. 9.50 mm) of length 10 mm with gap of 0.25 mm notched in the side. Microwaves were delivered to the resonator via a rigid coaxial cable with a loop (i.d. 9.00 mm) at the end. The outer shield of the coax cable was grounded to the larger copper tube (i.d. 13.90 mm o.d. 16.00 mm) that housed the entire ensemble and served as a microwave shield. To hold the copper tubes in place, a Rexolite pedestal and cap, milled to the same dimensions, were positioned above and below the copper inner tube within the larger shield to hold the resonator in place. An outer Rexolite housing held the entire assembly together and positions the height of the resonator correctly with respect to the cryostat optical windows. A 3 mm hole was drilled through the entire assembly to allow for optical excitation. The resonance frequency was adjusted by adding RF absorbing material (DigiKey 903−1506-ND) in the space between the two copper tubes.

Microwave pulses were generated using a Keysight M8190A Arbitrary Waveform Generator and sent through a Microwave Communications Laboratories, Inc. (MCLI) 18 GHz 10 dB attenuator to a Mini-Circuits HPA-100W-63+ High Power Amplifier. The amplified output was directed through a Mini-Circuits directional coupler (ZGDC35−93HP+) to monitor the waveform and then a MCLI isolator (IS-44) and circulator (CS-44) pair before being directed into the cryostat via an SMA connector (see Figure S30). The ADMR spectrum is the difference in the nsTA spectrum with the microwave pulses on and off.

https://doi.org/10.1021/acs.jpca.4c05015
J. Phys. Chem. A 2024, 128, 9371−9382

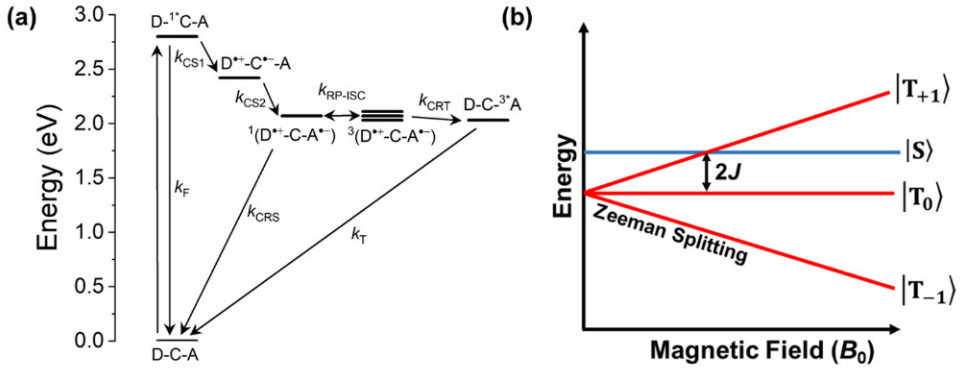

Figure 2. (a) Jablonski diagram detailing the energy levels of the D-C-A systems. The radical ion pair energies in toluene at 295 K and in PrCN at 85 K are similar. (b) Radical ion pair energy levels as a function of magnetic field ($2J > 0$).

EPR Spectroscopy. TREPR measurements at X-band were made using a Bruker Elexsys E580 EPR spectrometer equipped with a 3 mm split-ring resonator (ER4118X-MS3, Bruker) operating at ~9.6 GHz. The temperature was controlled by a continuous-flow optical cryostat (CF935, Oxford Instruments) using liquid nitrogen. Q-band measurements were performed on a lab-built instrument detailed previously[21] with several newer additions, namely, the digitizer has been upgraded to Acqiris SA220P DAQ card and the magnetic field was controlled with a Lakeshore F-41 Gmeter. The experiments were run with resonant frequencies of around 35 GHz using a Bridge12 loop-gap resonator (B12TQLP). The instrument was controlled with Specman4EPR, a commercially available control software.[36]

For EPR studies with light excitation, the sample was photoexcited at 415 nm with 7 ns pulses generated via an optical parametric oscillator (BasiScan, Spectra-Physics) pumped with the 355 nm output of a frequency-tripled Nd:YAG laser (Quanta-Ray Lab-150, Spectra-Physics) operating at a repetition rate of 10 Hz. The laser light was coupled into the resonator with a fiber optic cable, and the collimator was placed outside the resonator cryostat window. The laser power measured directly at the fiber optic output was 25 mW at 415 nm.

RESULTS AND DISCUSSION

Ground-State Absorption Spectroscopy. The ground-state absorption spectra of **MeOAn-ANI-NDI**, **MeOAn-ANI-xy-NDI**, **BDX-ANI-NDI**, and **BDX-ANI-xy-NDI** in toluene at 295 K and PrCN at 85 K are shown in Figure 1a,b, respectively. At both temperatures, the molecules without the xy spacer show ANI charge transfer bands that are red-shifted relative to those in which the xy group is present. This is attributed to the additional electron withdrawing effect of the electron deficient NDI acceptor on the ANI chromophore. In all cases, the ANI charge transfer band can be selectively excited at 415−420 nm.

Donor-Chromophore-Acceptor Energetics. The energies of the various charge-separated states in both 295 K toluene and in 85 K PrCN were determined using the methods reported earlier for **MeOAn-ANI-NDI** and **MeOAn-ANI-xy-NDI**.[27] The oxidation potential of BDX (0.78 V vs SCE[37]) is nearly identical to that of MeOAn (0.79 V vs SCE[27]) Moreover, the dielectric constants of toluene at 295 K (2.38) and PrCN at 85 K (2.3)[38] are nearly the same; thus, the radical ion pair energies for the molecules with the MeOAn and BDX donors are very similar, and are summarized in Figure 2a.

Application of a magnetic field to the SCRP results in Zeeman splitting of the SCRP triplet energy levels. Since the radical pair is produced initially in its singlet state, when the Zeeman splitting is larger than J, D, the differences between the g-factors of each radical and the differences in their total electron−nuclear hyperfine interactions, only $|S\rangle$ and $|T_0\rangle$ mix (Figure 2b).[28,39−42] When $2J > 0$, level crossing between $|S\rangle$ and $|T_{+1}\rangle$ occurs at $B = 2J$, which produces a resonance resulting from the increase in triplet radical pair yield at the crossing. This translates into a higher yield of ^{3}*NDI following charge recombination provided that $k_{CRT} > k_{CRS}$.

Charge-Transfer Dynamics. The charge separation and recombination dynamics of both **MeOAn-ANI-NDI** and **MeOAn-ANI-xy-NDI** following photoexcitation in toluene at 295 K have been reported previously.[27] Briefly, excitation of the ANI chromophore at 414 nm in **MeOAn-ANI-NDI** leads to rapid charge transfer to **MeOAn-ANI$^{+\bullet}$-NDI$^{-\bullet}$** with $k_{CS1} = (0.6 \pm 0.3\ \text{ps})^{-1}$. This process is distinguished by the loss of ^{1}*ANI stimulated emission at approximately 500 nm and the appearance of the characteristic NDI$^{\bullet-}$ features at 480, 610, 705, and 785 nm. Importantly, MeOAn$^{\bullet+}$ has no strong absorption bands in this region (Figure S1). The mechanistic preference for the ultrafast photooxidation of ANI results from strong electronic coupling between ANI and NDI that are directly linked by a N−N bond. This is followed by the second charge separation step to yield **MeOAn$^{\bullet+}$-ANI-NDI$^{\bullet-}$** with $k_{CS2} = (1.5 \pm 0.3\ \text{ps})^{-1}$, which then decays partially to the ^{3}*NDI triplet state with $k_{CR} = k_{CRS} + k_{CRT} = (28.0 \pm 0.6\ \text{ns})^{-1}$, with peaks at 454 and 488 nm (Figure S2).[43]

Photoexcited **MeOAn-ANI-xy-NDI** follows a different charge transfer pathway because the xylene bridge reduces the electronic coupling between ANI and NDI. The initial charge separation from ^{1}*ANI yields **MeOAn$^{\bullet+}$-ANI$^{\bullet-}$-xy-NDI** in $k_{CS1} = (7.9 \pm 0.3\ \text{ps})^{-1}$ in near-unity yield (Figure S3).[27] This is then followed by a charge shift to form **MeOAn$^{\bullet+}$-ANI-xy-NDI$^{\bullet-}$** in $k_{CS2} = (441 \pm 4\ \text{ps})^{-1}$. The **MeOAn$^{\bullet+}$-ANI-xy-NDI$^{\bullet-}$** SCRP recombines partially to ^{3}*NDI (Figure S4) in $k_{CR} = (240 \pm 1\ \text{ns})^{-1}$, which is considerably longer than **MeOAn$^{\bullet+}$-ANI-NDI$^{\bullet-}$**, once again, because the xylene spacer reduces the electronic coupling for this process.

The charge transfer dynamics of the MeOAn-containing triads have not been reported previously in solid solutions at cryogenic temperatures. In PrCN at 85 K, both compounds

https://doi.org/10.1021/acs.jpca.4c05015
J. Phys. Chem. A 2024, 128, 9371−9382

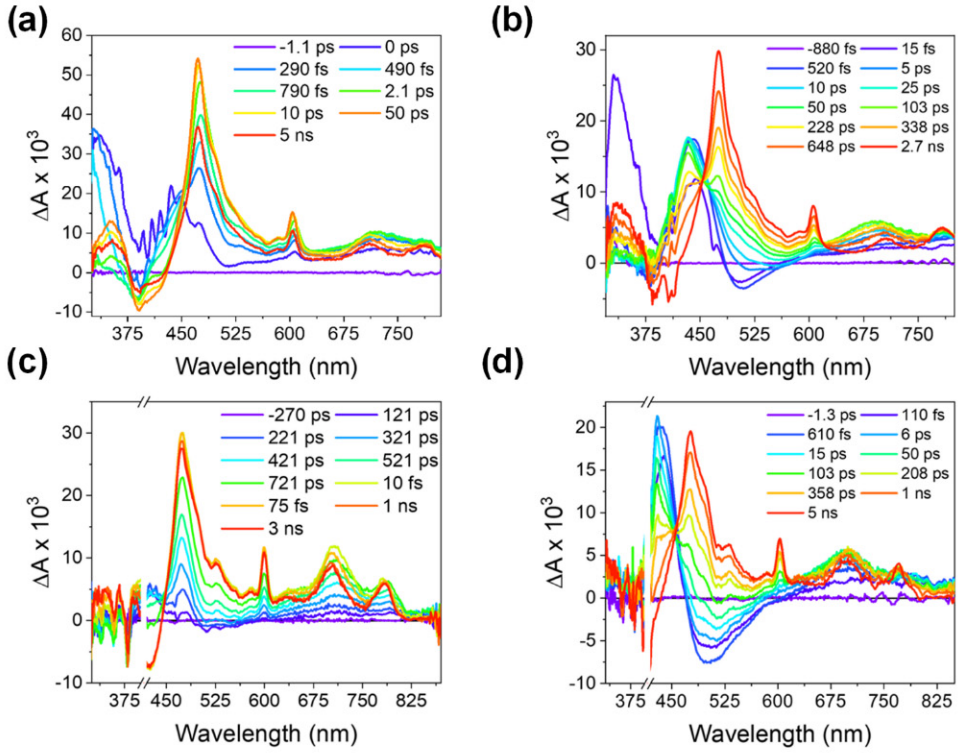

Figure 3. FsTA spectra (λ_{ex} = 414 nm). (a) **BDX-ANI-NDI** in toluene at 295 K (b) **BDX-ANI-xy-NDI** in toluene at 295 K, (c) **BDX-ANI-NDI** in PrCN at 85 K (d) **BDX-ANI-xy-NDI** in PrCN at 85 K.

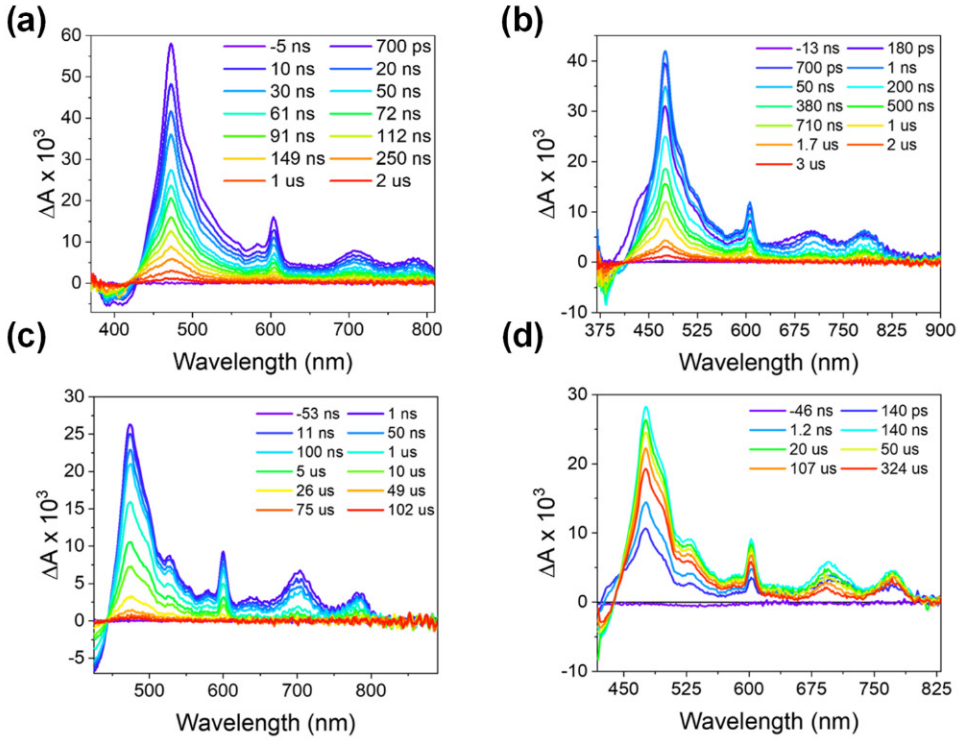

Figure 4. NsTA spectra (λ_{ex} = 414 nm). (a) **BDX-ANI-NDI** in toluene at 295 K (b) **BDX-ANI-xy-NDI** in toluene at 295 K, (c) **BDX-ANI-NDI** in PrCN at 85 K (d) **BDX-ANI-xy-NDI** in PrCN at 85 K.

follow the same charge transfer pathways as they do at 295 K. Moreover, the dielectric constant of frozen PrCN at 85 K is about 2.3,[38] which is very similar to that of toluene (2.38) at 295 K, so that the free energies of reaction should be very similar. There is an increased number of species in the fits of the low temperature data, indicating distributed kinetics in glassy PrCN at 85 K. Generally, the charge transfer rates decrease at low temperature because rotational relaxation of the donor and acceptor structures along the single bonds joining them results in smaller electronic coupling matrix

https://doi.org/10.1021/acs.jpca.4c05015
J. Phys. Chem. A 2024, 128, 9371−9382

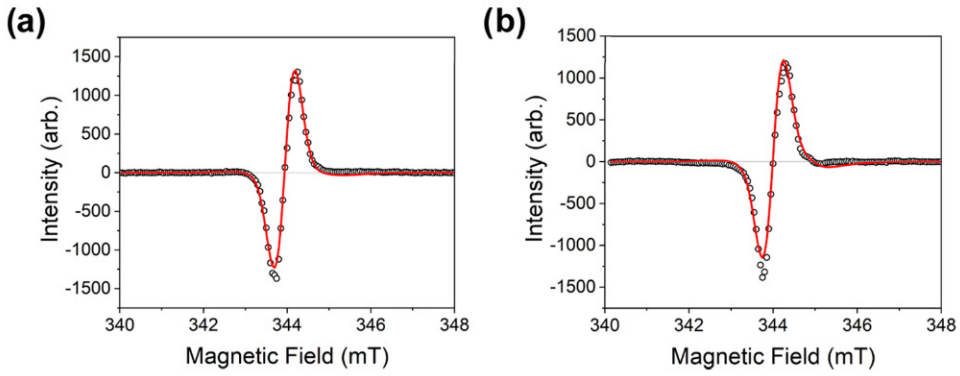

Figure 5. TREPR spectra (λ_{ex} = 414 nm) at 100 ns in PrCN at 85 K of **BDX-ANI-NDI** (a) and **BDX-ANI-xy-NDI** (b).

elements (V) for charge transfer.[44,45] This is reflected in the decreased J values at low temperatures, as discussed below, because $k_{CR} \propto J \propto V^2$.[46] The reaction **MeOAn−^{1}*ANI-NDI** → **MeOAn-ANI$^{\bullet+}$-NDI$^{\bullet-}$** occurs in <1 ps (Figure S5) and the transient spectrum is dominated by the NDI$^{\bullet-}$ features, which then decrease in magnitude slightly with k_{CS2} = (5.1 ± 0.2 ps)$^{-1}$ owing to the charge shift reaction **MeOAn-ANI$^{\bullet+}$-NDI$^{\bullet-}$** → **MeOAn$^{\bullet+}$-ANI-NDI$^{\bullet-}$**. The **MeOAn$^{\bullet+}$-ANI-NDI$^{\bullet-}$** SCRP then decays with k_{CR} = (72 ± 1 ns)$^{-1}$ with a small fraction recombining to form **MeOAn-ANI-^{3}*NDI** (Figure S6). For the corresponding molecule with the xylene bridge, the charge separation reaction **MeOAn−^{1}*ANI-xy-NDI**→ **MeOAn$^{\bullet+}$-ANI$^{\bullet-}$-xy-NDI** (Figure S7) occurs with k_{CS1} = (2.6 ± 0.3 ps)$^{-1}$. The ANI$^{-\bullet}$ state absorption at 420 nm appears with the loss of the stimulated emission, then decays as the charge shift reaction **MeOAn$^{\bullet+}$-ANI$^{\bullet-}$-xy-NDI** → **MeOAn$^{\bullet+}$-ANI-xy-NDI$^{\bullet-}$** occurs with k_{CS2} = (121 ± 2 ps)$^{-1}$, where the ANI$^{-\bullet}$ absorption features are replaced by those of NDI$^{-\bullet}$. The **MeOAn$^{\bullet+}$-ANI-xy-NDI$^{\bullet-}$** SCRP then decays with k_{CR} = (34 ± 1 μs)$^{-1}$ to give a low **MeOAn-ANI-xy-^{3}*NDI** yield (Figure S8).

Substituting BDX for MeOAn as the terminal hole acceptor in the triads once again does not result in significant changes in the free energies of the charge transfer reactions because these two donors have very similar oxidation potentials.[21] Also, much like MeOAn$^{\bullet+}$, BDX$^{\bullet+}$ has relatively weak absorption features in the visible spectrum, so that the transient absorption spectra are again dominated by those of ANI$^{\bullet-}$ and NDI$^{\bullet-}$. Following excitation of ANI at 414 nm, **BDX-ANI-NDI** rapidly forms **BDX-ANI$^{\bullet+}$-NDI$^{\bullet-}$**, which features a dominant NDI$^{\bullet-}$ band at 480 nm in k_{CS1} = (0.6 ± 0.3 ps)$^{-1}$ (Figures 3a and S9). The spectral features relax as the charge is transferred to BDX to form **BDX$^{\bullet+}$-ANI-NDI$^{\bullet-}$** in k_{CS2} = (8.4 ± 0.4 ps)$^{-1}$. This state then recombines mostly to the ground state in k_{CR} = (61 ± 1 ns)$^{-1}$, with a small fraction recombining to form **BDX-ANI-^{3}*NDI** (Figures 4a and S10).

In **BDX-ANI-xy-NDI** the initial charge transfer to form **BDX$^{\bullet+}$-ANI$^{\bullet-}$-xy-NDI** occurs in k_{CS1} = (15.0 ± 0.3 ps)$^{-1}$, with the ANI$^{-\bullet}$ absorption at 420 nm appearing prominently (Figures 3b and S11). Here, the rate constant for the second step to form **BDX$^{\bullet+}$-ANI-xy-NDI$^{\bullet-}$** is k_{CS2} = (445 ± 3 ps)$^{-1}$ and is comparable to that observed in **MeOAn$^{\bullet+}$-ANI-xy-NDI$^{\bullet-}$**. The terminal radical pair decays principally back to ground state with k_{CR} = (930 ± 4 ns)$^{-1}$ with the formation of a small yield of **BDX$^{\bullet+}$-ANI$^{\bullet-}$-xy-^{3}*NDI** (Figures 4b and S12).[28] Even though the charge separation rates for **BDX$^{\bullet+}$-ANI-xy-NDI$^{\bullet-}$** and **MeOAn$^{\bullet+}$-ANI-xy-NDI$^{\bullet-}$** are comparable, the charge recombination rate of the former is about four times slower than the latter.

Photoexcitation of **BDX-ANI-NDI** in PrCN at 85 K results in charge separation to form **BDX-ANI$^{\bullet+}$-NDI$^{\bullet-}$** in k_{CS1} = (0.4 ± 0.3 ps)$^{-1}$ similar to its behavior at 295 K, while the secondary charge separation to form **BDX$^{\bullet+}$-ANI-NDI$^{\bullet-}$** occurs in k_{CS2} = (11.6 ± 0.6 ps)$^{-1}$ (Figures 3c and S13), which decays in k_{CR} ∼ (10 μs)$^{-1}$ to reveal a low-amplitude feature that is likely due to **BDX-ANI-^{3}*NDI**, which decays in k_T = (60 ± 1 μs)$^{-1}$ (Figures 4c and S14). As stated above, there appears to be distributed kinetics in PrCN at 85 K. One potential explanation suggested by density functional theory (DFT) calculations is that the location of the electron density and therefore coupling of the radical pair is strongly dependent on the rotation of BDX about the single bond connecting it to the adjacent phenyl group. Additional consequences of this coupling are discussed below, but the presence of different conformations with distinct energies could contribute to the observed distributed kinetics.

The initial photodriven charge separation in **BDX-ANI-xy-NDI** yields **BDX$^{\bullet+}$-ANI$^{\bullet-}$-xy-NDI$^{\bullet-}$** with k_{CS1} = (16 ± 1 ps)$^{-1}$ at 85 K, while the secondary charge separation to form **BDX$^{\bullet+}$-ANI-xy-NDI$^{\bullet-}$** occurs in k_{CS2} = (370 ± 4 ps)$^{-1}$ (Figures 3d and S15), which is actually faster than the rate observed at 295 K, but slower than for **MeOAn-ANI-xy-NDI** at 85 K. **BDX$^{\bullet+}$-ANI-xy-NDI$^{\bullet-}$** persists beyond the 250 μs time window of the nsTA pump−probe delay limit and analysis of the nsTA data yields an estimate for k_{CR} = (1.5 ± 0.1 ms)$^{-1}$(Figures 4d and S16).

TREPR Spectroscopy. The TREPR spectra and T_m values of **BDX$^{\bullet+}$-ANI-NDI$^{\bullet-}$** and **BDX$^{\bullet+}$-ANI-xy-NDI$^{\bullet-}$** were determined to assess the potential of these SCRPs as spin qubit pairs. The TREPR spectra of **BDX$^{\bullet+}$-ANI-NDI$^{\bullet-}$** and **BDX$^{\bullet+}$-ANI-xy-NDI$^{\bullet-}$** were collected at X-band in PrCN at 85 K, and the spectra at 100 ns following the laser pulse are shown in Figure 5a,b, respectively. The spectra were simulated using the parameters given in Tables S1 and S2, respectively, The values of the spin−spin dipolar interaction (D) required to simulate the spectra yield SCRP distances based on the point dipole approximation for **BDX$^{\bullet+}$-ANI-NDI$^{\bullet-}$** and **BDX$^{\bullet+}$-ANI-xy-NDI$^{\bullet-}$** of 20 and 23 Å, respectively, and are in good agreement with the DFT-calculated distances for these compounds of 21.2 and 25.5 Å, respectively (Figure S25). Discrepancies between these values are likely due to the DFT distances being calculated using the optimized ground state geometry. To determine an accurate lifetime for **BDX$^{+\bullet}$-ANI-xy-NDI$^{-\bullet}$**, pulse-EPR measurements using the Hahn echo

https://doi.org/10.1021/acs.jpca.4c05015
J. Phys. Chem. A 2024, 128, 9371−9382

sequence ($h\nu$-T_{DAF}-$\pi/2$-τ-π-τ-echo) were conducted at different time delays between the initial laser pulse and the $\pi/2$ microwave pules (T_{DAF}), which yielded $k_{CR} \sim (550\ \mu s)^{-1}$ (Figure S17).

The same Hahn-echo pulse sequence was used to measure the SCRP phase memory time T_m by varying τ at a fixed T_{DAF} = 500 ns. Since **MeOAn$^{\bullet+}$-ANI-NDI$^{\bullet-}$** has the shortest SCRP lifetime, its spin echo intensity was insufficient to determine T_m. For all other compounds, the T_m values are given in Table 1 and the decay curves are given in Figures S18–S20. The data

Table 1. Summary of T_m Values

	MeOAN$^{+\bullet}$ or BDX$^{+\bullet}$ (μs)	NDI$^{-\bullet}$ (μs)	$\langle T_m \rangle$ (μs)
MeOAn-ANI-xy-NDI	1.86 ± 0.23	1.18 ± 0.22	1.51 ± 0.48
BDX-ANI-NDI	2.22 ± 0.18	1.61 ± 0.16	1.91 ± 0.43
BDX-ANI-xy-NDI	2.93 ± 0.1	2.77 ± 0.23	2.85 ± 0.11

show that substituting BDX for MeOAn increases T_m, which is most likely due to the decreased hyperfine interactions of BDX$^{\bullet+}$ relative to those of MeOAn$^{\bullet+}$. The increased T_m lifetimes demonstrate that reducing the electron–nuclear hyperfine splittings is an important design strategy for creating spin qubit pairs with increased coherence times.

The measured T_m values for **BDX-ANI-NDI** and **BDX-ANI-xy-NDI** compare favorably with those of other molecular systems. For example, we have measured T_m = 1.5 μs at 10 K for a covalently linked donor–acceptor(1)-acceptor(2) (D-A_1-A_2) molecule that uses fully deuterated *peri*-xanthenoxanthene (PXX) as D, naphthalenemonoimide (NMI) as A_1, and a C_{60} derivative as A_2.[47] Using that system, we have demonstrated both one- and two-qubit gate operations including the CNOT gate. We have also shown that singlet exciton fission can be used to generate four entangled spins that constitute a quintet spin state in a single crystal of 5,12-bis-(tricyclohexylsilylethynyl)tetracene, where T_m = 3.0 μs at 10 K.[48] In general, the $T_m \cong 3\ \mu s$ value for **BDX-ANI-xy-NDI** is significantly longer than the 10 ns microwave pulse duration typically used to manipulate the spin states (τ_{man}), thus allowing $T_m/\tau_{man} \cong 300$ operations to be performed before significant decoherence occurs. We and others have also shown that elimination of nuclear spins in the vicinity of the radicals can improve coherence times in both single spin and multispin systems.[15,49,50] All of these experiments are performed at temperatures above 4.2 K in condensed media, so that comparisons with other qubit technologies such as superconducting qubits[51] at millikelvin temperatures and trapped ions[52] at very low temperatures in vacuum are difficult. In the latter cases, spin coherence times are much longer due to the imposition of extreme conditions that shield the qubits from noise. Our goal in developing molecular qubits is to find ways to improve coherence times at higher temperatures in condensed media that afford sufficient isolation of the qubits to achieve practical T_m values for QIS applications such as sensing and coherent interprocessor communications in quantum devices.

Magnetic Field Effects (MFEs) on Triplet Yields Resulting from SCRP Recombination. There has been relatively little work on how magnetic field effects change with temperature, despite the fact that many spin properties relevant to potential QIS applications are enhanced at cryogenic temperatures. Furthermore, by studying the effect of temperature on J and D, it is possible to elucidate structural changes

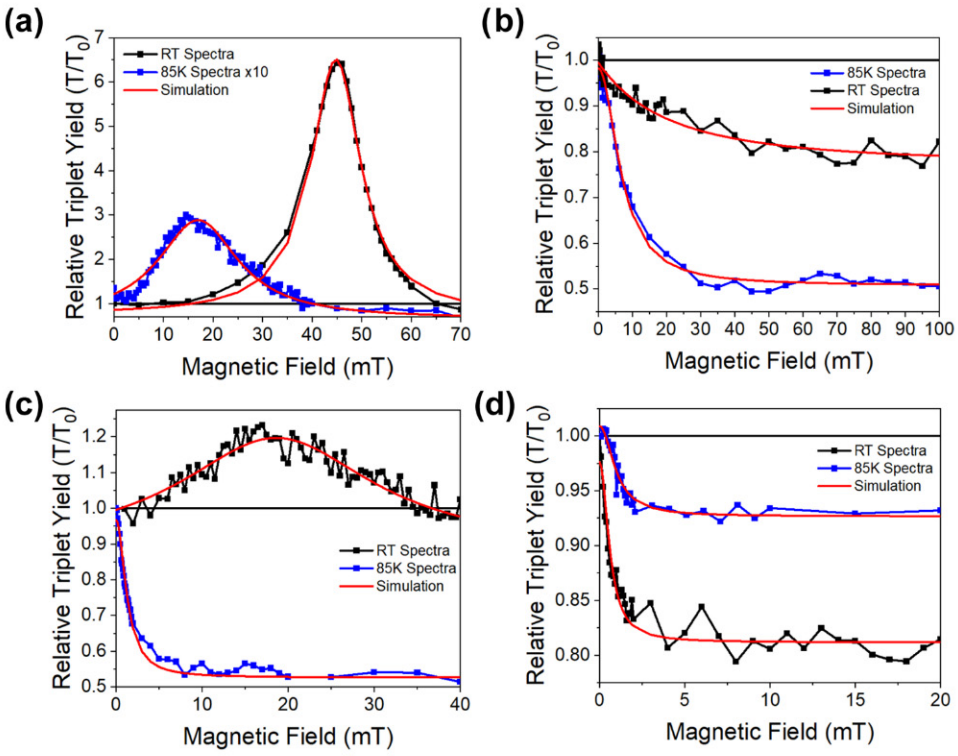

Figure 6. Magnetic field effects on the charge recombination triplet yield relative to B = 0. **MeOAn-ANI-NDI** (a), **MeOAn-ANI-xy-NDI** (b), **BDX-ANI-NDI** (c), and **BDX-ANI-xy-NDI** (d) in toluene at 295 K (black) and in PrCN at 85 K (blue) after excitation at 415 nm. Lorentzian fits are overlaid in red.

https://doi.org/10.1021/acs.jpca.4c05015
J. Phys. Chem. A 2024, 128, 9371–9382

and determine sources of motion and disorder within the molecule. The dependence of the triplet yield following SCRP recombination on an applied static magnetic field was determined for all four compounds in PrCN at 295 and 85 K (Figure 6). The nanosecond transient absorption spectra were monitored at times sufficiently long to ensure that maximal conversion of each SCRP to ^{3}*NDI had occurred. The nsTA difference spectra were integrated over 470−490 nm, where ^{3}*NDI absorbs, to obtain the ^{3}*NDI yield at a magnetic field B relative to that at zero magnetic field (T/T_0). Details of the data processing are given in the Supporting Information.

The MFEs on the yields of both **MeOAn-ANI-^{3}*NDI** and **MeOAn-ANI-xy-^{3}*NDI** at 295 K are in good agreement with previously published work (Figure 6a,b)[28] **MeOAn-ANI-NDI** exhibits a resonance at $2J$ = 45 mT with a full-width at half-maximum (fwhm) of 12.2 mT and about a 700% increase in ^{3}*NDI yield at the $|S\rangle$ - $|T_{+1}\rangle$ level crossing. At 85 K in PrCN, the $2J$ resonance for **MeOAn-ANI-NDI** decreases to 17 mT and is broader (fwhm = 19.7 mT) than at 295 K. The broadening likely derives from a distribution of J values that is a consequence of conformational changes within **MeOAn-ANI-NDI** upon cooling.[29] At 295 K, fast exchange occurs between the multiple conformers, leading to a narrowing of the resonance compared to 85 K. Similar effects were observed previously as a function of temperature in liquid solution, confirming that the MFE resonance is strongly sensitive to the details of molecular geometry.[29]

In contrast, J for **MeOAn-ANI-xy-NDI** is much smaller, showing no resonance, only a decrease in triplet yield as the magnetic field is increased. In this case, it is typical to quote the so-called $B_{1/2}$ value that is defined as the magnetic field at which half of the total triplet yield change has occurred. The value of $B_{1/2}$ expected from the electron−nuclear hyperfine splittings of radicals 1 and 2 can be calculated as a function of the total effective hyperfine interaction of all the nuclei within radicals 1 and 2, B_1 and B_2, respectively, that drive radical pair intersystem crossing as determined by eqs 1 and 2[53]

$$B_i = \sqrt{\sum_j I_{ij}(I_{ij}+1)a_{ij}^2} \quad (1)$$

$$B_{1/2} = \sqrt{3(B_1^2 + B_2^2)} \quad (2)$$

where i = 1 or 2, I is the nuclear spin quantum number and j is summed over all nuclear spins within radical i. Using eqs 1 and 2, and the hyperfine couplings of MeOAn$^{\bullet+}$, BDX$^{\bullet+}$, and NDI$^{\bullet-}$,[54] the estimated hyperfine contribution to $B_{1/2}$ is 4.5 mT for the MeOAn$^{\bullet+}$- NDI$^{\bullet-}$ SCRPs and is 0.7 mT for the BDX$^{\bullet+}$- NDI$^{\bullet-}$ SCRPs. Observed values of $B_{1/2}$ that are larger than the calculated $B_{1/2}$ values based solely on the hyperfine splittings of both radicals likely indicate the presence of multiple structural conformations, leading to a distribution of J values. In addition, changes in spin relaxation properties of the SCRP can result in significant changes to $B_{1/2}$ and the MFE line shape.[55−60]

For **MeOAn-ANI-xy-NDI** at 295 K $B_{1/2}$ = 12 mT, which is substantially larger than the hyperfine limited value of 4.5 mT and can be attributed to conformational changes that result in distributed J values.[55,61,62] For example, hindered rotation about the single bonds connecting the donors and acceptors as well as other motions may provide this additional source of distributed J values at 295 K. For **MeOAn-ANI-xy-NDI** in PrCN at 85 K, $B_{1/2}$ decreases to 8 mT as a consequence of conformational restrictions in the low temperature glass that result in a potentially narrower J distribution. The value of $B_{1/2}$ approaches more closely the 4.5 mT value expected from the hyperfine splittings alone.

As discussed previously, replacing the MeOAn group with BDX has two important ramifications in this context: (1) the radical ion pair distance increases and (2) the hyperfine interactions decrease. Based solely on the optimized ground-state distances for **BDX-ANI-NDI** (21.2 Å) and **BDX-ANI-xy-NDI** (25.5 Å) (Figure S25), J should be very small, and $B_{1/2}$ should approach 0.7 mT, its value due solely to the hyperfine interactions. However, these predictions are only partially borne out in the data, indicating that structural changes have significant contributions.

The MFE for **BDX-ANI-NDI** in toluene at 295 K exhibits a very broad resonance at $2J$ = 18.6 mT with a fwhm = 27.8 mT (Figure 6c). This indicates an increase in the J distribution and/or the spin relaxation contribution to the MFE line width relative to those of **MeOAn-ANI-NDI**, which have been attributed earlier to conformational changes in the piperazine ring.[29] Here, DFT calculations were used to determine the distribution of the BDX$^{\bullet+}$ spin density as a function of the dihedral angle of the BDX group with respect to the adjacent phenyl group (Figures 7 and S27−28). Both relaxed and frozen potential energy surface scans along this internal molecular coordinate show that as the dihedral angle approaches 90°, spin density delocalizes from the BDX onto the adjacent phenyl group, effectively decreasing the distance between the radicals, which increases their electronic coupling and J value. It is important to note that these potential energy surface scans predict an energy barrier of 3−4 kcal/mol, which can be overcome at room temperature. Thus, the breadth of the observed J resonance at room temperature indicates that the distribution of BDX-phenyl dihedral angles is also broad, resulting in differing spin distributions between BDX and the phenyl linked to it.

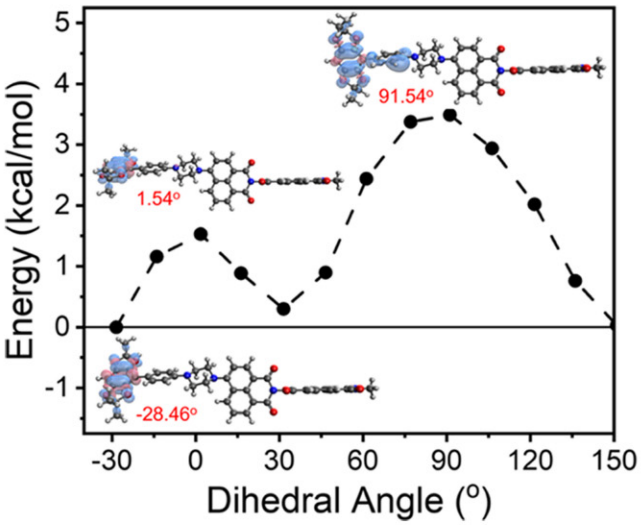

Figure 7. Frozen potential energy surface scan of **BDX$^{\bullet+}$-ANI- NDI** along the BDX-phenyl dihedral angle as defined in Figure S26. The spin density distributions at key inflection points are shown.

The MFE for **BDX-ANI-NDI** exhibits a dramatic temperature dependence with the 18.6 mT resonance at 295 K

https://doi.org/10.1021/acs.jpca.4c05015
J. Phys. Chem. A 2024, 128, 9371−9382

collapsing at 85 K to yield $B_{1/2}$ = 2.7 mT (Figure 6c), which is much narrower than what is observed using the MeOAn donor. The structural changes that lead to increased coupling at 295 K are diminished greatly at 85 K, indicating that the dihedral angle between the BDX group and adjacent phenyl remains closer to the equilibrium geometry. The spin density remains localized on the BDX in the lowest energy geometries (Figure 7). In comparison, $B_{1/2}$ = 2.4 mT for **BDX-ANI-xy-NDI** in toluene at 295 K and drops to $B_{1/2}$ = 1.3 mT at 85 K (Figure 6d), which is smaller than that of the analogous **MeOAn-ANI-xy-NDI**. The $B_{1/2}$ value for **BDX-ANI-xy-NDI** at 85 K closely approaches $B_{1/2}$ = 0.7 mT determined by hyperfine coupling alone. This result suggests that the conformational mobility of **BDX-ANI-xy-NDI** at 85 K is very limited resulting in a narrow J distribution.

Absorption Detected Magnetic Resonance (ADMR) Spectroscopy. The results presented above for the **BDX-ANI-NDI** and **BDX-ANI-xy-NDI** SCRPs show that they have long lifetimes, enhanced T_m values, and significant MFEs at low temperatures, which make them potentially useful spin qubit pairs. However, an important additional criterion is establishing a means of optical readout of the spin states. Optical readout can provide both higher sensitivity and selectivity than microwave readout in a conventional pulse-EPR measurement. To demonstrate optical read out, the transient absorption spectrum of **BDX-ANI-^{3}*NDI** produced by radical pair recombination was monitored with and without a 1 μs, 2.79 GHz, microwave pulse applied 1 μs after the laser pulse. The resulting difference spectrum is shown in Figure 8.

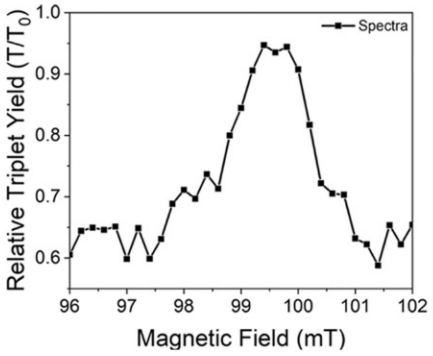

Figure 8. ADMR spectrum of **BDX-ANI-NDI** in PrCN at 85 K (λ_{ex} = 414 nm).

The presence of the long microwave pulse causes a resonance in the relative **BDX-ANI-^{3}*NDI** yield centered at B_0 = 99.5 mT, consistent with the g-factor of its SCRP precursor. The long microwave pulse saturates the transitions between the mixed $|S\rangle$ and $|T_0\rangle$ sublevels and $|T_{\pm1}\rangle$ leading to an increase in **BDX-ANI-^{3}*NDI** yield because $k_{CRT} > k_{CRS}$ (Figure 2a). In fact, the triplet yield nearly returns to the levels seen at resonance in the MFE at $|S\rangle - |T_{+1}\rangle$ level crossing (Figure 2b). The relative triplet yield baseline is slightly higher in this measurement, but this is likely due to noise in the baseline that varies slightly between measurements. Regardless, the application of the microwave pulse is approximately 85% efficient at regenerating the triplet population. This is a promising start, and future work will focus on applying shorter microwave pulses to perform more complex gate operations and applying fluorescence detection to probe smaller ensembles with the goal of eventually achieving single molecule detection. This experiment is also possible for **BDX-ANI-xy-NDI**; however, the 1 kHz laser repetition rate will need to be reduced significantly so that **BDX$^{\bullet+}$-ANI-xy-NDI$^{\bullet-}$** recovers fully to its ground state in between laser excitation pulses to optimize signal averaging. Work in this direction is proceeding.

CONCLUSIONS

The four compounds examined here provide a design strategy for optimizing both charge transfer rates and J values in SCRPs for potential applications in QIS. We have demonstrated that **BDX-ANI-NDI** and **BDX-ANI-xy-NDI** have enhanced SCRP lifetimes and spin coherence times. Moreover, we have shown that structural changes upon cooling in a glassy solvent to cryogenic temperatures greatly reduces the J values of these systems. In addition, we have demonstrated optical read out of the SCRP spin states in **BDX-ANI-NDI**, which is essential for reducing ensemble sizes. The combination of these features makes **BDX-ANI-NDI** and **BDX-ANI-xy-NDI** exciting candidates for future QIS studies.

ASSOCIATED CONTENT

Supporting Information

The Supporting Information is available free of charge at https://pubs.acs.org/doi/10.1021/acs.jpca.4c05015.

Synthesis and characterization of all compounds, additional fsTA and ns TA data, TREPR spectra, data used to determine T_m, additional MFE data and fitting details, DFT calculations, and instrumental description (PDF)

AUTHOR INFORMATION

Corresponding Authors

Ryan M. Young − *Department of Chemistry, Center for Molecular Quantum Transduction, and Paula M. Trienens Institute for Sustainability and Energy, Northwestern University, Evanston, Illinois 60208-3113, United States;* orcid.org/0000-0002-5108-0261; Email: ryan.young@northwestern.edu

Michael R. Wasielewski − *Department of Chemistry, Center for Molecular Quantum Transduction, and Paula M. Trienens Institute for Sustainability and Energy, Northwestern University, Evanston, Illinois 60208-3113, United States;* orcid.org/0000-0003-2920-5440; Email: m-wasielewski@northwestern.edu

Authors

Paige J. Brown − *Department of Chemistry, Center for Molecular Quantum Transduction, and Paula M. Trienens Institute for Sustainability and Energy, Northwestern University, Evanston, Illinois 60208-3113, United States;* orcid.org/0000-0002-2934-0098

Yunfan Qiu − *Department of Chemistry, Center for Molecular Quantum Transduction, and Paula M. Trienens Institute for Sustainability and Energy, Northwestern University, Evanston, Illinois 60208-3113, United States;* orcid.org/0000-0002-4666-1424

Elisabeth I. Latawiec − *Department of Chemistry, Center for Molecular Quantum Transduction, and Paula M. Trienens Institute for Sustainability and Energy, Northwestern University, Evanston, Illinois 60208-3113, United States*

Brian T. Phelan − *Department of Chemistry, Center for Molecular Quantum Transduction, and Paula M. Trienens Institute for Sustainability and Energy, Northwestern University, Evanston, Illinois 60208-3113, United States;* orcid.org/0000-0002-5849-0319

Nikolai A. Tcyrulnikov − *Department of Chemistry, Center for Molecular Quantum Transduction, and Paula M. Trienens Institute for Sustainability and Energy, Northwestern University, Evanston, Illinois 60208-3113, United States*

Jonathan R. Palmer − *Department of Chemistry, Center for Molecular Quantum Transduction, and Paula M. Trienens Institute for Sustainability and Energy, Northwestern University, Evanston, Illinois 60208-3113, United States*

Matthew D. Krzyaniak − *Department of Chemistry, Center for Molecular Quantum Transduction, and Paula M. Trienens Institute for Sustainability and Energy, Northwestern University, Evanston, Illinois 60208-3113, United States;* orcid.org/0000-0002-8761-7323

Sebastian M. Kopp − *Department of Chemistry, Center for Molecular Quantum Transduction, and Paula M. Trienens Institute for Sustainability and Energy, Northwestern University, Evanston, Illinois 60208-3113, United States;* orcid.org/0000-0003-0324-6404

Yuheng Huang − *Department of Chemistry, Center for Molecular Quantum Transduction, and Paula M. Trienens Institute for Sustainability and Energy, Northwestern University, Evanston, Illinois 60208-3113, United States*

Complete contact information is available at: https://pubs.acs.org/10.1021/acs.jpca.4c05015

Notes

The authors declare no competing financial interest.

■ ACKNOWLEDGMENTS

This work was supported by the National Science Foundation under award no. CHE-2154627 (M.R.W., synthesis, transient optical and EPR measurements). This research was also supported as part of the Center for Molecular Quantum Transduction, an Energy Frontier Research Center funded by the U.S. Department of Energy (DOE), Office of Science, Basic Energy Sciences (BES), under award DE-SC0021314 (R.M.Y. transient optical measurements and M.D.K., EPR data analysis). The authors thank Dr. Stephen A. Miller of the Northwestern University Laser and Electronics Design Core Facility (NU-LED) for instrumentation development assistance and the Northwestern Research Shop for resonator fabrication. ^{1}H nuclear magnetic resonance (NMR) spectroscopy, and mass spectrometry are conducted in IMSERC facilities at Northwestern University, which have received support from the Soft and Hybrid Nanotechnology Experimental (SHyNE) Resource (NSF ECCS-2025633), NSF CHE-1048773, Northwestern University, the State of Illinois, and the International Institute for Nanotechnology (IIN).

■ REFERENCES

(1) Gaita-Ariño, A.; Luis, F.; Hill, S.; Coronado, E. Molecular spins for quantum computation. *Nat. Chem.* **2019**, *11*, 301−309.

(2) Harrow, A. W.; Montanaro, A. Quantum computational supremacy. *Nature* **2017**, *549*, 203−209.

(3) Biamonte, J.; Wittek, P.; Pancotti, N.; Rebentrost, P.; Wiebe, N.; Lloyd, S. Quantum machine learning. *Nature* **2017**, *549*, 195−202.

(4) Awschalom, D. D.; Hanson, R.; Wrachtrup, J.; Zhou, B. B. Quantum technologies with optically interfaced solid-state spins. *Nat. Photonics* **2018**, *12*, 516−527.

(5) Degen, C. L.; Reinhard, F.; Cappellaro, P. Quantum sensing. *Rev. Mod. Phys.* **2017**, *89*, No. 035002.

(6) Kimble, H. J. The quantum internet. *Nature* **2008**, *453*, 1023−1030.

(7) Wasielewski, M. R.; Forbes, M. D. E.; Frank, N. L.; Kowalski, K.; Scholes, G. D.; Yuen-Zhou, J.; Baldo, M. A.; Freedman, D. E.; Goldsmith, R. H.; Goodson, T.; Kirk, M. L.; McCusker, J. K.; Ogilvie, J. P.; Shultz, D. A.; Stoll, S.; Whaley, K. B. Exploiting chemistry and molecular systems for quantum information science. *Nat. Rev. Chem.* **2020**, *4*, 490−504.

(8) Aromí, G.; Aguilà, D.; Gamez, P.; Luis, F.; Roubeau, O. Design of magnetic coordination complexes for quantum computing. *Chem. Soc. Rev.* **2012**, *41*, 537−546.

(9) Atzori, M.; Sessoli, R. The second quantum revolution: Role and challenges of molecular chemistry. *J. Am. Chem. Soc.* **2019**, *141*, 11339−11352.

(10) Moreno-Pineda, E.; Godfrin, C.; Balestro, F.; Wernsdorfer, W.; Ruben, M. Molecular spin qudits for quantum algorithms. *Chem. Soc. Rev.* **2018**, *47*, 501−513.

(11) Troiani, F.; Affronte, M. Molecular spins for quantum information technologies. *Chem. Soc. Rev.* **2011**, *40*, 3119−3129.

(12) Schäfter, D.; Wischnat, J.; Tesi, L.; De Sousa, J. A.; Little, E.; McGuire, J.; Mas-Torrent, M.; Rovira, C.; Veciana, J.; Tuna, F.; Crivillers, N.; van Slageren, J. Molecular one- and two-qubit systems with very long coherence times. *Adv. Mater.* **2023**, *35*, No. 2302114.

(13) Bayliss, S. L.; Laorenza, D. W.; Mintun, P. J.; Kovos, B. D.; Freedman, D. E.; Awschalom, D. D. Optically addressable molecular spins for quantum information processing. *Science* **2020**, *370*, 1309−1312.

(14) DiVincenzo, D. P. The physical implementation of quantum computation. *Fortschr. Phys.* **2000**, *48*, 771−783.

(15) Qiu, Y. F.; Eckvahl, H. J.; Equbal, A.; Krzyaniak, M. D.; Wasielewski, M. R. Enhancing coherence times of chromophore-radical molecular qubits and qudits by rational design. *J. Am. Chem. Soc.* **2023**, *145*, 25903−25909.

(16) Harvey, S. M.; Wasielewski, M. R. Photogenerated spin-correlated radical pairs: From photosynthetic energy transduction to quantum information science. *J. Am. Chem. Soc.* **2021**, *143*, 15508−15529.

(17) Mani, T. Molecular qubits based on photogenerated spin-correlated radical pairs for quantum sensing. *Chem. Phys. Rev.* **2022**, *3*, No. 021301.

(18) Childress, L.; Dutt, M. V. G.; Taylor, J. M.; Zibrov, A. S.; Jelezko, F.; Wrachtrup, J.; Hemmer, P. R.; Lukin, M. D. Coherent dynamics of coupled electron and nuclear spin qubits in diamond. *Science* **2006**, *314*, 281−285.

(19) Bourassa, A.; Anderson, C. P.; Miao, K. C.; Onizhuk, M.; Ma, H.; Crook, A. L.; Abe, H.; Ul-Hassan, J.; Ohshima, T.; Son, N. T.; Galli, G.; Awschalom, D. D. Entanglement and control of single nuclear spins in isotopically engineered silicon carbide. *Nat. Mater.* **2020**, *19*, 1319−1325.

(20) Xie, F.; Mao, H.; Lin, C.; Feng, Y.; Stoddart, J. F.; Young, R. M.; Wasielewski, M. R. Quantum sensing of electric fields using spin-correlated radical ion pairs. *J. Am. Chem. Soc.* **2023**, *145*, 14922−14931.

(21) Rugg, B. K.; Krzyaniak, M. D.; Phelan, B. T.; Ratner, M. A.; Young, R. M.; Wasielewski, M. R. Photodriven quantum teleportation of an electron spin state in a covalent donor−acceptor−radical system. *Nat. Chem.* **2019**, *11*, 981−986.

(22) Nelson, J. N.; Zhang, J.; Zhou, J.; Rugg, B. K.; Krzyaniak, M. D.; Wasielewski, M. R. CNOT gate operation on a photogenerated molecular electron spin-qubit pair. *J. Chem. Phys.* **2020**, *152*, No. 014503.

(23) Olshansky, J. H.; Zhang, J.; Krzyaniak, M. D.; Lorenzo, E. R.; Wasielewski, M. R. Selectively addressable photogenerated spin qubit pairs in DNA hairpins. *J. Am. Chem. Soc.* **2020**, *142*, 3346−3350.

(24) Olshansky, J. H.; Krzyaniak, M. D.; Young, R. M.; Wasielewski, M. R. Photogenerated spin-entangled qubit (radical) pairs in DNA hairpins: Observation of spin delocalization and coherence. *J. Am. Chem. Soc.* **2019**, *141*, 2152−2160.
(25) Lorenzo, E. R.; Olshansky, J. H.; Abia, D. S. D.; Krzyaniak, M. D.; Young, R. M.; Wasielewski, M. R. Interaction of photogenerated spin qubit pairs with a third electron spin in DNA hairpins. *J. Am. Chem. Soc.* **2021**, *143*, 4625−4632.
(26) Olshansky, J. H.; Harvey, S. M.; Pennel, M. L.; Krzyaniak, M. D.; Schaller, R. D.; Wasielewski, M. R. Using photoexcited core/shell quantum dots to spin polarize appended radical qubits. *J. Am. Chem. Soc.* **2020**, *142*, 13590−13597.
(27) Greenfield, S. R.; Svec, W. A.; Gosztola, D.; Wasielewski, M. R. Multistep photochemical charge separation in rod-like molecules based on aromatic imides and diimides. *J. Am. Chem. Soc.* **1996**, *118*, 6767−6777.
(28) Weiss, E. A.; Ratner, M. A.; Wasielewski, M. R. Direct measurement of singlet-triplet splitting within rodlike photogenerated radical ion pairs using magnetic field effects: Estimation of the electronic coupling for charge recombination. *J. Phys. Chem. A* **2003**, *107*, 3639−3647.
(29) Weiss, E. A.; Tauber, M. J.; Ratner, M. A.; Wasielewski, M. R. Electron spin dynamics as a probe of molecular dynamics: Temperature-dependent magnetic field effects on charge recombination within a covalent radical ion pair. *J. Am. Chem. Soc.* **2005**, *127*, 6052−6061.
(30) Huang, Y.; Krzyaniak, M. D.; Young, R. M.; Wasielewski, M. R. Mechanistic study of electron spin polarization transfer in covalent donor-acceptor-radical systems. *Appl. Magn. Reson.* **2022**, *53*, 949−961.
(31) Schweiger, A.; Jeschke, G. *Principles of Pulse Electron Paramagnetic Resonance*, 1st ed.; Oxford University Press, USA: Oxford, 2001; p 578.
(32) Chen, H.-F.; Gardner, D. M.; Carmieli, R.; Wasielewski, M. R. Controlling the orientation of spin-correlated radical pairs by covalent linkage to nanoporous anodic aluminum oxide membranes. *Chem. Commun.* **2013**, *49*, 8614−8616.
(33) Young, R. M.; Dyar, S. M.; Barnes, J. C.; Juricek, M.; Stoddart, J. F.; Co, D. T.; Wasielewski, M. R. Ultrafast conformational dynamics of electron transfer in exbox^{4+}⊂perylene. *J. Phys. Chem. A* **2013**, *117*, 12438−12448.
(34) Hardy, W. N.; Whitehead, L. A. Split-ring resonator for use in magnetic resonance from 200−2000 MHz. *Rev. Sci. Instrum.* **1981**, *52*, 213−216.
(35) Froncisz, W.; Hyde, J. S. The loop-gap resonator: A new microwave lumped circuit ESR sample structure. *J. Magn. Reson.* **1982**, *47*, 515−521.
(36) Epel, B.; Gromov, I.; Stoll, S.; Schweiger, A.; Goldfarb, D. Spectrometer manager: A versatile control software for pulse EPR spectrometers. *Concepts Magn. Reson.: Magn. Reson. Eng.* **2005**, *26B*, 36−45.
(37) Carmieli, R.; Mi, Q.; Ricks, A. B.; Giacobbe, E. M.; Mickley, S. M.; Wasielewski, M. R. Direct measurement of photoinduced charge separation distances in donor-acceptor systems for artificial photosynthesis using OOP-ESEEM. *J. Am. Chem. Soc.* **2009**, *131*, 8372−8373.
(38) Mao, H.; Young, R. M.; Krzyaniak, M. D.; Wasielewski, M. R. Controlling the dynamics of three electron spin qubits in a donor-acceptor-radical molecule using dielectric environment changes. *J. Phys. Chem. Lett.* **2021**, *12*, 2213−2218.
(39) Closs, G. L.; Forbes, M. D. E.; Norris, J. R. Spin-polarized electron-paramagnetic resonance-spectra of radical pairs in micelles - observation of electron spin-spin interactions. *J. Phys. Chem. A* **1987**, *91*, 3592−3599.
(40) Buckley, C. D.; Hunter, D. A.; Hore, P. J.; McLauchlan, K. A. Electron spin resonance of spin-correlated radical pairs. *Chem. Phys. Lett.* **1987**, *135*, 307−312.
(41) Timmel, C. R.; Till, U.; Brocklehurst, B.; McLauchlan, K. A.; Hore, P. J. Effects of weak magnetic fields on free radical recombination reactions. *Mol. Phys.* **1998**, *95*, 71−89.
(42) Tait, C. E.; Krzyaniak, M. D.; Stoll, S. Computational tools for the simulation and analysis of spin-polarized EPR spectra. *J. Magn. Reson.* **2023**, *349*, No. 107410.
(43) Wu, Y.; Nalluri, S. K. M.; Young, R. M.; Krzyaniak, M. D.; Margulies, E. A.; Stoddart, J. F.; Wasielewski, M. R. Charge and spin transport in an organic molecular square. *Angew. Chem., Int. Ed.* **2015**, *54*, 11971−11977.
(44) Marcus, R. A. On the theory of electron-transfer reactions. VI. Unified treatment for homogeneous and electrode reactions. *J. Chem. Phys.* **1965**, *43*, 679−701.
(45) Ulstrup, J.; Jortner, J. Effect of intramolecular quantum modes on free energy relations for electron transfer reactions. *J. Chem. Phys.* **1975**, *63*, 4358−4368.
(46) Kobori, Y.; Sekiguchi, S.; Akiyama, K.; Tero-Kubota, S. Chemically induced dynamic electron polarization study on the mechanism of exchange interaction in radical ion pairs generated by photoinduced electron transfer reactions. *J. Phys. Chem. A* **1999**, *103*, 5416−5424.
(47) Mao, H.; Pažèra, G. J.; Young, R. M.; Krzyaniak, M. D.; Wasielewski, M. R. Quantum gate operations on a spectrally addressable photogenerated molecular electron spin-qubit pair. *J. Am. Chem. Soc.* **2023**, *145*, 6585−6593.
(48) Jacobberger, R. M.; Qiu, Y.; Williams, M. L.; Krzyaniak, M. D.; Wasielewski, M. R. Using molecular design to enhance the coherence time of quintet multiexcitons generated by singlet fission in single crystals. *J. Am. Chem. Soc.* **2022**, *144*, 2276−2283.
(49) Yu, C.-J.; Graham, M. J.; Zadrozny, J. M.; Niklas, J.; Krzyaniak, M. D.; Wasielewski, M. R.; Poluektov, O. G.; Freedman, D. E. Long coherence times in nuclear spin-free vanadyl qubits. *J. Am. Chem. Soc.* **2016**, *138*, 14678−14685.
(50) Zadrozny, J. M.; Niklas, J.; Poluektov, O. G.; Freedman, D. E. Millisecond coherence time in a tunable molecular electronic spin qubit. *ACS Cent. Sci.* **2015**, *1*, 488−492.
(51) Devoret, M. H.; Schoelkopf, R. J. Superconducting circuits for quantum information: An outlook. *Science* **2013**, *339*, 1169−1174.
(52) Monroe, C.; Kim, J. Scaling the ion trap quantum processor. *Science* **2013**, *339*, 1164−1169.
(53) Weller, A.; Nolting, F.; Staerk, H. A quantitative interpretation of the magnetic field effect on hyperfine-coupling-induced triplet formation from radical ion pairs. *Chem. Phys. Lett.* **1983**, *96*, 24−27.
(54) Colvin, M. T.; Carmieli, R.; Miura, T.; Richert, S.; Gardner, D. M.; Smeigh, A. L.; Dyar, S. M.; Conron, S. M.; Ratner, M. A.; Wasielewski, M. R. Electron spin polarization transfer from photogenerated spin-correlated radical pairs to a stable radical observer spin. *J. Phys. Chem. A* **2013**, *117*, 5314−5325.
(55) Steiner, U. E.; Schäfer, J.; Lukzen, N. N.; Lambert, C. J-resonance line shape of magnetic field-affected reaction yield spectrum from charge recombination in a linked donor−acceptor dyad. *J. Phys. Chem. C* **2018**, *122*, 11701−11708.
(56) Steiner, U. E.; Ulrich, T. Magnetic-field effects in chemical-kinetics and related phenomena. *Chem. Rev.* **1989**, *89*, 51−147.
(57) Miura, T.; Murai, H. Real-time observation of the spin-state mixing process of a micellized radical pair in weak magnetic fields by nanosecond fast field switching. *J. Phys. Chem. A* **2008**, *112*, 2526−2532.
(58) Maeda, K.; Miura, T.; Arai, T. A practical simulation and a novel insight to the magnetic field effect on a radical pair in a micelle. *Mol. Phys.* **2006**, *104*, 1779−1788.
(59) Miura, T.; Scott, A. M.; Wasielewski, M. R. Electron spin dynamics as a controlling factor for spin-selective charge recombination in donor-bridge-acceptor molecules. *J. Phys. Chem. C* **2010**, *114*, 20370−20379.
(60) Miura, T.; Carmieli, R.; Wasielewski, M. R. Time-resolved EPR studies of charge recombination and triplet-state formation within donor-bridge-acceptor molecules having wire-like oligofluorene bridges. *J. Phys. Chem. A* **2010**, *114*, 5769−5778.

https://doi.org/10.1021/acs.jpca.4c05015
J. Phys. Chem. A 2024, 128, 9371−9382

(61) Klein, J. H.; Schmidt, D.; Steiner, U. E.; Lambert, C. Complete monitoring of coherent and incoherent spin flip domains in the recombination of charge-separated states of donor-iridium complex-acceptor triads. *J. Am. Chem. Soc.* **2015**, *137*, 11011−11021.
(62) Fay, T. P.; Manolopoulos, D. E. Radical pair intersystem crossing: Quantum dynamics or incoherent kinetics? *J. Chem. Phys.* **2019**, *150*, No. 151102.

https://doi.org/10.1021/acs.jpca.4c05015
J. Phys. Chem. A 2024, 128, 9371−9382